

# Temperature-Programmed Hydrogenation (TPH) and in Situ Mössbauer Spectroscopy Studies of Carbonaceous Species on Silica-Supported Iron Fischer–Tropsch Catalysts<sup>†</sup>

Jian Xu and Calvin H. Bartholomew\*

Catalysis Laboratory and Department of Chemical Engineering, Brigham Young University, Provo, Utah 84602

Received: March 17, 2004; In Final Form: July 8, 2004

Carbonaceous surface species and bulk iron carbides formed under realistic Fischer–Tropsch synthesis (FTS) conditions on moderately dispersed, active silica-supported iron catalysts (Fe/SiO<sub>2</sub>, FePt/SiO<sub>2</sub>, and FePtK/SiO<sub>2</sub>) were characterized. Bulk iron phase compositions were determined by Mössbauer spectroscopy and phase transformations of carbonaceous species during pretreatment with CO, H<sub>2</sub>, or H<sub>2</sub>/CO and following reaction were characterized using temperature-programmed hydrogenation (TPH). Isothermal transient rates of FTS were also measured for catalysts after different pretreatments. Six surface and bulk carbonaceous species were quantitatively identified from combined TPH and Mössbauer spectra of the FePtK catalyst. They include, in order of decreasing reactivity, (a) adsorbed, atomic carbon; (b) amorphous, lightly polymerized hydrocarbon or carbon surface species; (c) bulk  $\epsilon'$  and  $\chi$  carbides (Fe<sub>2.2</sub>C and Fe<sub>2.5</sub>C); and (d) disordered and moderately ordered graphitic surface carbons. A correlation between the amount of reactive  $\alpha$ -carbon (C <sub>$\alpha$</sub> ) and initial catalytic activity was established. The method of Li et al.<sup>1</sup> for measuring irreversible chemisorption of CO does not appear to provide quantitative measurements of active site densities on silica-supported iron. Models, based on this and previous work, are proposed for iron phase and carbon phase transformations in silica-supported iron during pretreatment, FTS, and postreaction passivation/oxidation.

## 1. Introduction

Iron-based catalysts are preferred to cobalt-based counterparts in Fischer–Tropsch synthesis (FTS) of hydrocarbons from coal- or biomass-derived synthesis gas because of their lower cost, lower methane selectivity, lower sensitivity to poisons, flexible product slate, and robustness at low H<sub>2</sub>/CO ratios (enabled by high activity for production of H<sub>2</sub> via the water-gas-shift reaction).<sup>2–15</sup> However, the use of conventional, precipitated Fe catalysts in the most economical reactors, slurry bubble columns, has been limited by their low structural integrity; i.e., unsupported, precipitated iron catalysts undergo attrition at high rates to fine particles (approximately micrometer diameter or smaller), leading to uneconomical loss of the catalyst, high slurry viscosity, and difficulty in separating catalyst particles from the wax product.<sup>9,13,16–19</sup> These observed high rates of attrition are in large part chemically induced due to volumetric changes during the transformation of Fe<sub>3</sub>O<sub>4</sub> to iron carbides, evident by the sprouting of carbide “buds” (small crystallites or nodules) at the surface of larger magnetite crystallites; under the mechanical stress of slurry circulation these carbide nodules split off readily to form submicrometer particles.<sup>16,17</sup> Since active, selective, attrition-resistant supported cobalt catalysts have been developed for slurry FT processes, it should be in principle possible to develop attrition-resistant supported iron catalysts of high activity and selectivity using methods similar to those applied to cobalt catalysts. Indeed, selected silica and alumina carriers,<sup>18</sup> spray-dried precipitated iron catalysts containing more than 9–10% silica,<sup>17</sup> and silica- or alumina-supported iron catalysts<sup>13</sup> are found to have high attrition resistance relative to unsupported, precipitated iron catalysts.

Nevertheless, activities and liquid/wax selectivities of supported iron catalysts<sup>3,13,20–22</sup> are generally lower and methane selectivity unacceptably higher than those of unsupported, precipitated iron catalysts. This can be in large part attributed to strong interactions of iron oxides with silica and alumina carriers<sup>20–22</sup> which (1) limit formation of the active carbide phase and (2) produce new acid sites at the iron–support interface that catalyze alternate routes to the formation of methane.<sup>23</sup> Nevertheless, it should be possible to avoid these problems through careful treatment of the support surface,<sup>21</sup> incorporation of additives such as Cu that facilitate reduction of iron oxides,<sup>14,15</sup> and addition of basic promoters such as K<sub>2</sub>O.

In a recent companion study<sup>24</sup> we undertook the design of a supported Pt- and K-promoted Fe catalyst based on principles generally employed in the preparation and design of cobalt catalysts. Three silica-supported catalysts, unpromoted, Pt-promoted, and Pt/K-promoted, each containing 10 wt % iron, were prepared, characterized and tested using a statistically designed set of experiments. The preparation involved a novel acetone-phase evaporative deposition of dehydrated iron nitrate onto an attrition-resistant silica carrier that had been dehydroxylated at high temperature. Following pretreatment in H<sub>2</sub>, CO, or H<sub>2</sub>/CO the Pt/K-promoted catalyst was found to be well-reduced, moderately well-dispersed, highly active for production of C<sub>2+</sub> hydrocarbons—clearly more so than previously reported for supported iron—and at surprisingly low Fe and K loadings. Of course, it was desirable to understand why. In initial attempts to correlate activity with chemical and physical properties it was found that activities for the Fe and Fe/Pt catalysts correlate well with chi carbide content measured by Mössbauer spectroscopy following 120 h of reaction; however, in the case of the Pt/K-promoted catalyst no such correlation was apparent. It was concluded in agreement with others<sup>10,14</sup> that a correlation of activity with bulk iron composition should be unlikely;

\* To whom correspondence should be addressed. E-mail: bartc@byu.edu. Tel.: 801-422-4162. Fax: 801-422-0151.

<sup>†</sup> Part of the special issue “Michel Boudart Festschrift”.

**TABLE 1: Forms and Reactivities of Carbon Species Formed in CO Hydrogenation on Iron**

structural type	designation	peak temperature (°C) for reaction with H <sub>2</sub>	references
1. adsorbed, atomic carbon; surface carbide	$\alpha$	270–390	25, 27, 28, 29, 33, PW <sup>a</sup>
2. polymeric, amorphous aggregates			
a. polymethylene	$\beta_1$	420–455	31–33, PW
b. disordered polymeric carbon	$\beta_2$		
3. iron carbides			
a. $\epsilon'$ (Fe <sub>2.0</sub> 2C)	$\gamma_1$	480–597	33, PW
b. $\chi$ (Fe <sub>2.5</sub> C)	$\gamma_2$	517–688	
4. graphitic (crystalline) films			
a. semi-ordered sheets	$\delta_1$	600–700	16, 29, 33, PW
b. moderately ordered sheets	$\delta_2$	650–750	

<sup>a</sup> PW = present work.

instead, the possibility of establishing a correlation of active surface carbon species coverage with activity was considered. For this purpose, a study of surface and bulk carbons using temperature-programmed reaction methods and in situ Mössbauer spectroscopy was considered.

It is of great practical importance in the design of Fe FT catalysts to obtain a specific knowledge of carbon species deposited during different pretreatments and under industrial FTS conditions. Temperature-programmed surface reaction of H<sub>2</sub> (TPH) and O<sub>2</sub> (TPO) with adsorbed and/or bulk carbons has been used effectively for identification of carbon species of different structures and reactivities on Ni, Fe, and Ru catalysts,<sup>25–33</sup> including (1) adsorbed, atomic surface carbon, (2) polymeric, amorphous carbon, (3) vermicular (filamentous) carbon, (4) iron or nickel carbides, and (5) graphitic carbon. In a previous TPH study in our laboratory<sup>33</sup> these species (except for filamentous carbon), including two iron carbides and two forms of graphite carbon, were observed in TPH studies of unsupported Fe and Fe/K catalysts after in situ reaction at 215–245 °C, 1 atm, and H<sub>2</sub>/CO = 1. In a study of supported iron catalysts, at least five different forms of carbonaceous materials were identified by FTIR and TPO on Fe/silica after 260 h of reaction (300 °C, 15 atm, H<sub>2</sub>/CO = 1), including aliphatic, aromatic, and oxygenated hydrocarbons and carbidic and amorphous carbons. The distribution of these species was found to vary with support.<sup>32</sup> Table 1 summarizes and briefly describes more common forms of carbon and carbides observed in used iron FT catalysts.

There is to our knowledge no previously published TPH study of the effects of in situ pretreatment and reaction at high-pressure conditions which quantitatively address carbon speciation and species transformations in iron FT catalysts.

Mössbauer absorption spectroscopy (MABs) is a proven, effective technique for in situ investigation of different heterogeneous catalysts and a powerful tool for studying catalyst structure–activity relationships.<sup>34</sup> While it is generally a tool for bulk analysis (like XRD), MABs may be used to study surface atoms of well-dispersed bimetallic clusters that are too small for conventional X-ray diffraction analysis.<sup>35</sup> In situ Mössbauer spectroscopy has been successfully applied in a large number of studies to the characterization of iron FT catalysts at various stages of carburization. For example, Bianchi et al.<sup>36</sup> reported that bulk iron was 74% carburized to a mixture of  $\epsilon'$ -(Fe<sub>2.2</sub>C) and  $\chi$ -(Fe<sub>2.5</sub>C), the carbides building up more slowly than surface carbon species. In situ Mössbauer analysis of a 2% Pt–Fe/SiO<sub>2</sub> catalyst<sup>37</sup> suggested that iron carbide is probably formed in a separate phase from either Pt or PtFe alloy. These isolated Fe ensembles after carburizing could contribute to the high hydrocarbon productivity of this catalyst.<sup>37</sup>

The objective of this work was to study the transformations of surface carbons and surface/bulk iron carbide species in well-

dispersed, silica-supported Fe, FePt, and FePtK catalysts. Effects of pretreatment atmosphere, duration, and reaction time on these carbon species were studied using the following:

a. TPH with on-line mass spectrometry for identification of carbonaceous materials on the surface of iron catalysts, isothermal transient measurements of FTS rate and selectivity, and CO chemisorption/desorption to measure active site density.

b. High-pressure in situ Mössbauer spectroscopy to determine bulk phase transformation of iron FTS catalysts (changes in surface species could not be observed since Fe dispersion was only 10%) after pretreatment and reaction at industrially relevant FTS conditions.

## 2. Experimental Section

**Catalyst Synthesis.** Evaporative deposition from acetone solution of dehydrated iron nitrate was used in the preparation of three iron catalysts: 10% Fe–90% SiO<sub>2</sub>, 10% Fe–1.0% Pt–89% SiO<sub>2</sub>, and 10% Fe–1.0% Pt–0.2% K–88.8% SiO<sub>2</sub> (wt %; henceforth designated as Fe, FePt, and FePtK). Details of this preparation were described in a previous paper.<sup>24</sup> The catalyst carrier was a silica gel (Davisil 644) dried at 600 °C for 24 h. Fe(NO<sub>3</sub>)<sub>3</sub>·9H<sub>2</sub>O was dried at 80 °C for 24 h to remove most of the water of hydration. A slurry of the dried Fe(NO<sub>3</sub>)<sub>3</sub> and Davisil 644 support with HPLC-grade acetone was transferred into a flask and stirred. Some of the dissolved iron reacted with the solvent to form a brown precipitate, which was filtered out. Helium gas was bubbled through the slurry until the acetone had evaporated. The wet catalyst paste was oven-dried to a powder at 80 °C for 24 h and stored in a desiccator. Similarly, Pt-promoted and Pt-plus K-promoted catalyst were prepared by adding the required amount of acetone-dissolved Pt amine salt (in the case of the FePtK catalyst, potassium nitrate was added in water solution) to the calcined Fe catalyst.

**Temperature-Programmed Surface Reaction-Mass Spectrometry (TPSR-MS).** A TPSR system with on-line mass spectrometry was used for TPH, isothermal transient, and CO TPD measurements.<sup>24,38</sup> Gaseous feeds were controlled and metered using mass flow controllers. Gases were purified using an Alltech Oxytrap to remove oxygen and a zeolite trap to remove water. The outlet of the microreactor was connected to a quadrupole mass spectrometer through a capillary inlet system. The temperature of the reactor was controlled by an OMEGA 4200 temperature controller giving a linear increase in temperature in the range of 1–400 K/min.

**TPH Experiments.** Two sets of experiments were conducted on 10 wt % Fe/1% Pt/0.2% K/SiO<sub>2</sub>: (1) TPH spectra were obtained after pretreatment in H<sub>2</sub>, syngas (H<sub>2</sub>/CO = 1.0), or CO at 280 °C and 1 atm for 16 h followed by reaction for 10 h at  $T = 265$  °C and  $P = 10$  atm in H<sub>2</sub>/CO = 1.0 and (2) TPH spectra were obtained after pretreatment in 20% CO/He or

syngas ( $H_2/CO = 1.0$ ) at 280 °C and 1 atm for 1, 2, 6, or 16 h in separate runs.

In each TPH experiment 50 mg of calcined catalyst was loaded into a stainless steel cell followed by purging in helium for 30 min. The temperature was then increased to 280 °C at a ramp of 1 °C/min, following which a flow of pretreatment gas at 1 atm was introduced and the reactor temperature was held at 280 °C for a specified period; for catalyst samples in the first set of experiments the temperature was reduced to 265 °C following which the reaction was carried out for 10 h. Following pretreatment (and reaction—in the first set of experiments), the catalyst was cooled in 50 sccm argon to room temperature and the gas was switched to 50 sccm  $H_2$  at 1 atm while the temperature was increased to 800 °C at 35 °C/min.  $CH_4$  was monitored using mass signals ( $m/z$ ) of 15 ( $CH_3$  fragments of  $CH_4$ ) instead of 16 to avoid the interference of water vapor and  $CO_2$  cracking.<sup>39</sup> Deconvolution and analysis of TPH spectra for individual peak positions and areas were performed for each spectrum using the SOLVER tool in Excel.

**Isothermal Transient Measurements of FTS Rates.** Initial rates of FTS were also measured using on-line mass spectroscopy. Fifty milligrams of catalyst was loaded into the stainless steel microreactor. Catalyst samples were pretreated at 1 atm separately in each of the following procedures:

1. CO Pretreatment: Samples were treated in 20% CO/He (10 sccm CO in 40 sccm He), ramped at 5 °C/min to 280 °C, held for 1 h, and then cooled to 265 °C in 40 sccm He.

2.  $H_2$  Pretreatment: Samples were treated in 60 sccm  $H_2$ , ramped at 5 °C/min to 280 °C, held for 1 h, and cooled to 265 °C in 40 sccm He.

3. He Pretreatment: Samples were treated in 40 sccm He, ramped at 5 °C/min to 280 °C, held for 1 h, and cooled to 265 °C in 40 sccm He.

Following these pretreatments, samples were exposed to synthesis gas ( $H_2/CO/Ar = 1:1:0.1$ , 1 atm, 64 sccm). The transient evolution of reduction—carburization products ( $CH_4$ ,  $H_2O$ , and  $CO_2$ , etc.) at 265 °C was monitored as a function of time.

**Temperature-Programmed Desorption (TPD-CO) for Irreversibly Chemisorbed CO Site Density Measurement.** CO chemisorption uptake measurements were divided into two steps: the first step was a pretreatment/reaction in either CO or synthesis gas ( $H_2/CO = 1.0$ ); the second step was the TPD-CO experiment.

(1) *Pretreatment/Reaction.* 0.1–0.2 g of calcined catalyst was purged in argon for 30 min, followed by switching to a stream of 50 sccm pretreatment gas (CO/Ar stream 20/80 mol %, syngas of  $H_2/CO = 50/50$  mol % or pure  $H_2$ ) at 1 atm. The temperature was then increased to 280 °C at 5 °C/min and held at 280 °C for 1 h. Following this carburization/reaction step, the catalyst was purged at this temperature in argon for 1 h to remove reversibly adsorbed species and then cooled to room temperature for subsequent CO active site density measurements.

(2) *Temperature-Programmed Desorption (TPD-CO).* CO TPD measurements of CO site density consisted of two steps denoted here as TPD1 and TPD0, respectively. In TPD1, CO adsorption on the pretreated sample was carried out by passing a stream of 20% CO/Ar at 50 sccm through the catalyst bed at room temperature and 1 atm for one-half hour. The physisorbed CO species was then removed by purging the sample in argon for 0.5 h. Finally, a TPD was carried out by heating the catalyst to 800 °C at 1 atm and 35 °C/min. Evolving CO and  $CO_2$  were monitored using their mass signals ( $m/z$ ) of 28 and 44, respectively. In the second step (TPD0) the sample procedures

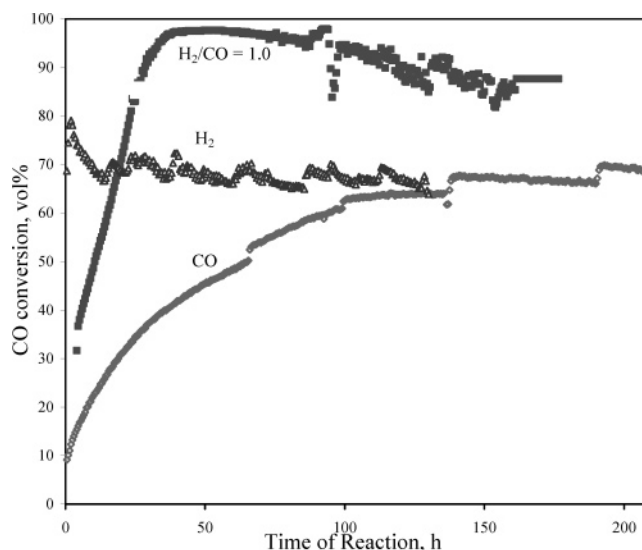


**Figure 1.** Effects of pretreatment on conversion versus time behavior of 10%Fe1.0Pt/0.2K/SiO<sub>2</sub> at 265 °C and 10 atm after pretreatments in CO,  $H_2$ , and syngas ( $H_2/CO = 1$ ) conducted at 280 °C.

in TPD1 were followed except for the CO adsorption step. Irreversibly chemisorbed CO was found from the difference between peak areas under the two curves (TPD1–TPD0). This method for determining irreversibly chemisorbed CO was reported to measure active sites formed during pretreatment (carburization/reduction) and FTS reaction on unsupported iron catalysts and should in principle apply to supported iron catalysts.<sup>1,40</sup>

**Mössbauer Spectroscopy.** (1) *On Spent Catalyst after Fixed Bed Activity Tests.* A 0.3 g sample of passivated catalyst was pressed to a 1 in. diameter wafer and placed in a Plexiglas cell. Mössbauer spectra of fresh and spent, passivated catalysts, were collected at 298 K using an Austin S-600 spectrometer system with a laser absolute velocity calibrator that enables peak positions to be determined to within  $\pm 0.01$  mm/s. The  $\gamma$ -ray source was  $^{57}Co$  in a rhodium matrix. Peak positions and isomer shifts of all spectra are reported with respect to metallic iron.

(2) *In Situ High-Pressure Mössbauer Spectroscopy.* A low-pressure, controlled-atmosphere cell was used in previous studies.<sup>41</sup> It was improved in this study by adding two newly designed O-ring-sealed Mylar windows pressurized by reactant gas on both sides of each window. This unique design enables use of Mylar windows for high pressures while significantly reducing cell construction and maintenance costs and avoiding use of toxic, expensive Beryllium. Following different pretreatments according to procedures described in the previous section, high-pressure in situ Mössbauer spectra were collected in  $H_2/CO = 1.0$  at 280 °C for different durations and exposure to typical FTS conditions, e.g., 10 atm, 265 °C, and  $H_2/CO = 1.0$ .

### 3. Results

**Temperature-Programmed Surface Reaction-Mass Spectrometry (TPSR-MS).** (1) *TPH.* In our previous study,<sup>24</sup> activity-time performance for FePtK/SiO<sub>2</sub> was found to vary greatly with pretreatment environment. Data in Figure 1 from that study show that initial activities of FePtK catalyst decrease in the order of decreasing hydrogen content of the pretreatment gas, i.e.,  $H_2$ ,  $H_2/CO$ , and CO. To further understand this catalytic behavior, carbonaceous surface species in FePtK/SiO<sub>2</sub> were studied by TPH after 16 h of pretreatment in  $H_2$ , CO, or  $H_2/CO$  followed by 10 h of reaction. TPH spectra showing methane evolution rate (due to reaction of carbon with  $H_2$ ) for samples



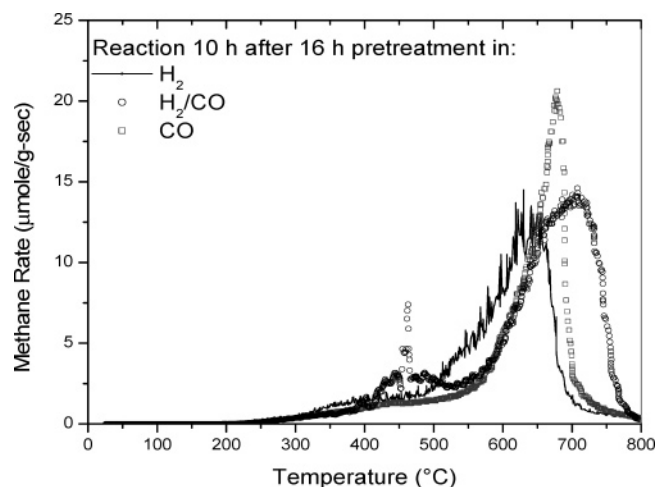


**Figure 2.** TPH spectra of 10 wt % Fe/1% Pt/0.2% K/SiO<sub>2</sub> after pretreatment in H<sub>2</sub>, syngas (H<sub>2</sub>/CO = 1.0), or CO at 280 °C for 16 h followed by 10 h of reaction ( $T = 265$  °C,  $P = 10$  atm in H<sub>2</sub>/CO = 1.0).

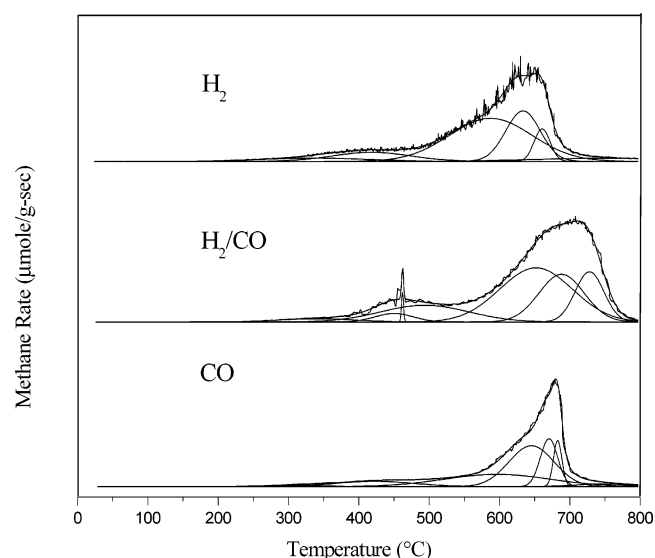


**Figure 3.** TPH spectra of 10 wt % Fe/1% Pt/0.2% K/SiO<sub>2</sub> after pretreatment in H<sub>2</sub>, syngas, or CO followed by reaction showing individual peak contributions from the various carbon species.

pretreated in each of the three gases are plotted together in Figure 2, while corresponding deconvoluted spectra are shown in Figure 3, and an enlarged section which includes peaks for  $\alpha$ -carbon is shown in Figure 4. Peak temperatures, equivalent carbon monolayer numbers, and fractional peak areas are tabulated in Table 2.

From the data in Figures 2 and 3 it is evident that the temperature of the most intense peak (around 600–700 °C) increases in the order H<sub>2</sub>, CO, and H<sub>2</sub>/CO, corresponding to a decrease in carbon reactivity. For samples pretreated in H<sub>2</sub> and CO followed by reaction, only one intense peak appears at 620 and 670 °C, respectively, while for the sample pretreated in H<sub>2</sub>/CO followed by 10 h of synthesis, an additional low-intensity peak is evident at 460 °C. Shifts in peak temperature with pretreatment environment are also evident in individual peak contributions of various carbon species obtained from deconvoluted spectra (Figure 3 and Table 2A). A method for quantitative analysis of overlapping TPH peaks for unpromoted and K-promoted Fe FT catalyst was reported by Eliason and Bartholomew.<sup>33</sup> Their spectra were fitted with Gaussian curves

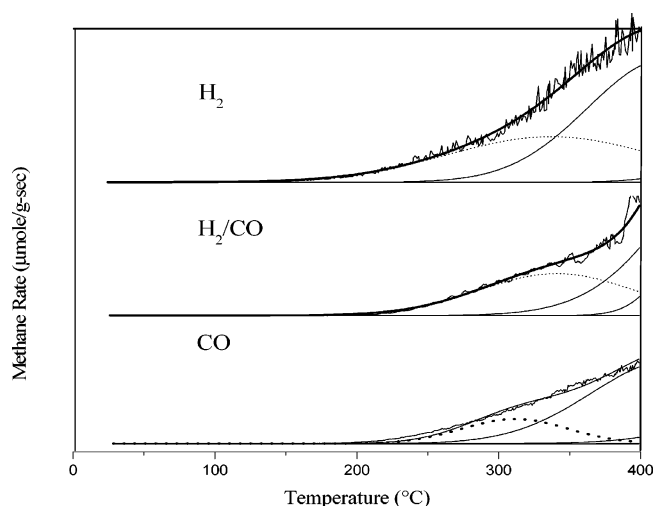


**Figure 4.** Enlarged sections of Figure 3 showing C<sub>α</sub> peaks as dotted lines.

**TABLE 2: Results of Temperature-Programmed Surface Reaction (TPH) of H<sub>2</sub> with Carbonaceous Species on 10 wt % Fe/1% Pt/0.2% K/SiO<sub>2</sub> after Pretreatment in H<sub>2</sub>, H<sub>2</sub>/CO, or CO for 16 h at 280 °C Followed by 10 h of Reaction at 265 °C**

A. TPH Peak Temperatures (°C)						
pretreatment	carbide	amorphous	carbide		graphitic	
gas	$\alpha$	$\beta$	$\gamma_1$	$\gamma_2$	$\delta_1$	$\delta_2$
H <sub>2</sub>	337	418	588	633	661	747
H <sub>2</sub> /CO	341	456	573	688	728 <sup>a</sup>	
CO	311	423	597	658	683	748
B. Monolayer Carbon Equivalents of Peak Areas						
pretreatment	carbide	amorphous	carbide		graphitic	
gas	$\alpha$	$\beta$	$\gamma_1$	$\gamma_2$	$\delta_1$	$\delta_2$
H <sub>2</sub>	1.1	2.2	10.8	5.3	1.6	0.9
H <sub>2</sub> /CO	0.8	2.4	13.8	6.4	4.3	
CO	0.3	1.8	5.4	11.2	1.6	0.6
C. Percentage Compositions of Carbon Species						
pretreatment	carbide	amorphous	carbide		graphitic	
gas	$\alpha$	$\beta$	$\gamma_1$	$\gamma_2$	$\delta_1$	$\delta_2$
H <sub>2</sub>	4.8	9.9	50	24	7.2	4.2
H <sub>2</sub> /CO	2.6	8.4	48	22	15	
CO	1.6	8.5	26	53	7.8	2.7

<sup>a</sup> Graphitic carbon of reactivity between  $\delta_1$  and  $\delta_2$ .

to yield up to seven peaks, designated as  $\alpha_1$ ,  $\alpha_2$ ,  $\beta$ ,  $\gamma_1$ ,  $\gamma_2$ ,  $\delta_1$ , and  $\delta_2$  (consistent with the nomenclature in Table 1).

Observed peak temperatures and their assignments to these same carbon species are listed in Table 2A for samples of Fe–Pt–K/silica after each of the three pretreatments. These spectra were best fitted by six peaks assigned to  $\alpha$ ,  $\beta$ ,  $\gamma_1$ ,  $\gamma_2$ ,  $\delta_1$ , and  $\delta_2$  species; as indicated in Table 1,  $\alpha$ ,  $\beta$ ,  $\gamma$ , and  $\delta$  species are assigned to adsorbed, atomic carbon, amorphous surface methylene chains or films, bulk iron carbide, and graphitic carbon. Peak temperatures increase in that same order, i.e., in order of decreasing reactivity with H<sub>2</sub>. The peak temperature assignments for these species are based on previous literature and, in the case of the carbides, are correlated with compositions determined from Mössbauer spectroscopy.

Table 2B lists the area under each curve in terms of carbon monolayer equivalents based upon iron metal area. The corresponding percentage compositions of carbon species are given in Table 2C. The carbon monolayer equivalents for  $\alpha$ -carbon

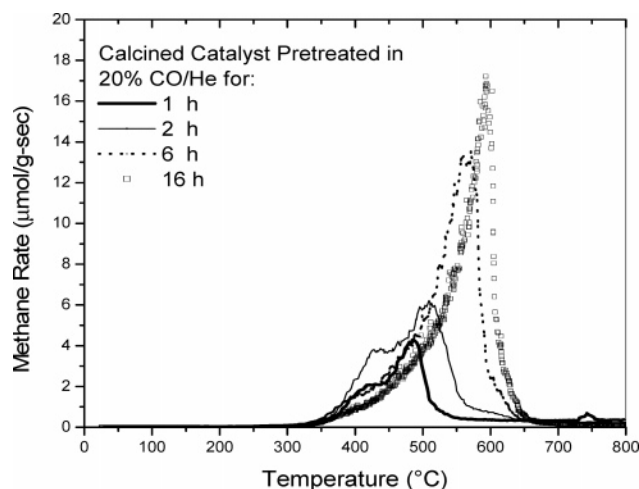


**Figure 5.** TPH spectra of 10 wt % Fe/1% Pt/0.2% K/SiO<sub>2</sub> after pretreatment in 20% CO/He at 280 °C for 1, 2, 6, and 16 h, respectively.

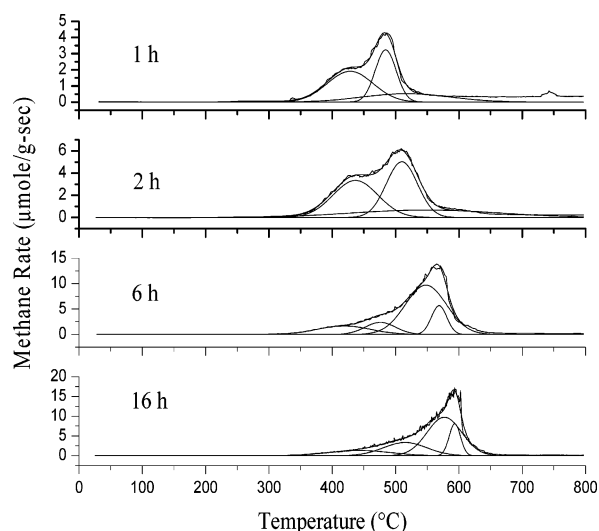


**Figure 6.** TPH spectra showing individual peak contributions from the various carbon species (10 wt % Fe/1% Pt/0.2% K/SiO<sub>2</sub> after different durations of pretreatment in 20% CO/He at 280 °C).

(the most reactive carbon form) decrease in the order of pretreatment by H<sub>2</sub> (1.1 monolayers), H<sub>2</sub>/CO (0.8 monolayers), and CO (0.3 monolayers) (corresponding peak areas are shown by dotted lines in Figure 4). This is the same order for initial catalyst activity from Figure 1. Beta carbons range from 1 to 2 monolayers, while carbides ( $\gamma_1$  plus  $\gamma_2$ ) range from 16 to 20 equivalent monolayers, this latter large number being roughly consistent with the quantity of carbon predicted for bulk carbide observed by Mössbauer spectroscopy. The quantity of high-temperature graphitic carbons varies from 2 to 4 monolayers. The extent of carburization in terms of total equivalent carbon monolayers decreases in the order of H<sub>2</sub>/CO pretreated (28.6 layers) > H<sub>2</sub> pretreated (21.8 layers) > CO pretreated (20.9 layers).

Effects of pretreatment duration were studied for the same FePtK catalyst pretreated in 20% CO/He at 280 °C. TPH with hydrogen was carried out following 1, 2, 6, and 16 h pretreatments (Figure 5). The four spectra from Figure 5 are deconvoluted in Figure 6 with enlarged sections in Figure 7 revealing little or no C<sub>α</sub>. Peak temperatures, equivalent carbon monolayers, and percentage peak areas are tabulated in Table 3.

It is evident in Figure 5 that methane peak maxima increase in intensity and progressively shift to higher temperatures with increasing pretreatment duration. Optimal fits in the deconvolu-

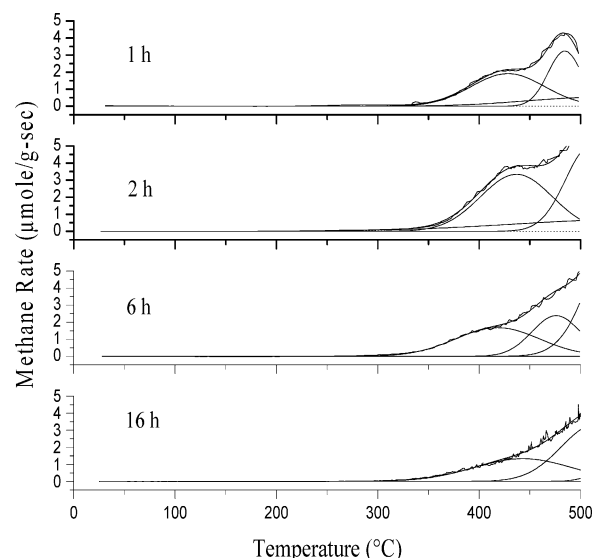


**Figure 7.** Enlarged sections of Figure 6 showing C<sub>α</sub> peaks as dotted lines.

**TABLE 3: TPH Peak Temperatures for Various Carbon Species on 10 wt % Fe/1% Pt/0.2% K/SiO<sub>2</sub> as a Function of Duration of Pretreatment in 20% CO/He at 280 °C**

A. TPH Peak Temperatures (°C)				
pretreatment time (h)	carbidec $\alpha$	amorphous $\beta$	carbide $\gamma_1$ $\gamma_2$	
1	285	428	484	517
2	274	434	510	548
6		418	512	569
16		443	515	585

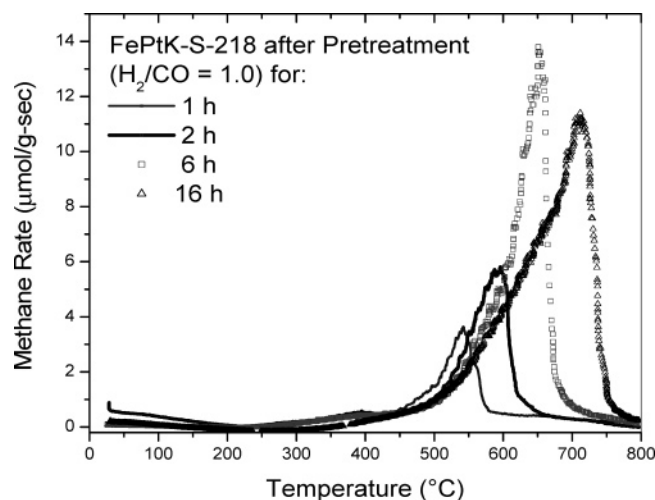
  

B. Monolayer Carbon Equivalents of Peak Areas				
pretreatment time (h)	$\alpha$	$\beta$	$\gamma_1$	$\gamma_2$
1	0.10	2.8	2.2	1.5
2	0.03	4.8	5.1	3.2
6		2.9	9.1	8.8
16		2.7	10.2	8.4

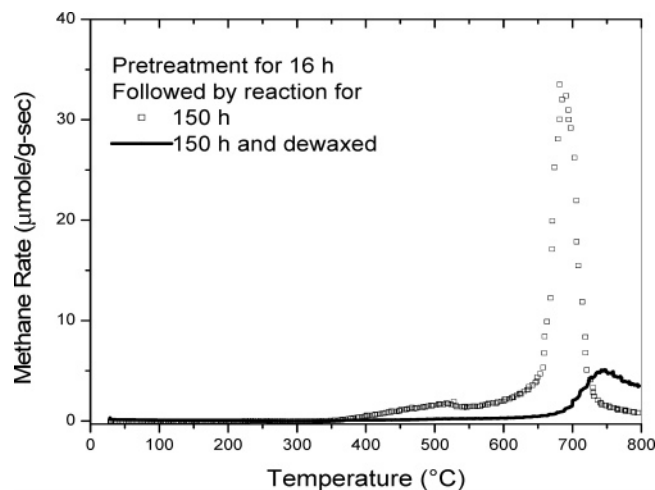
  

C. Percentage Compositions of Carbon Species				
pretreatment time (h)	$\alpha$	$\beta$	$\gamma_1$	$\gamma_2$
1	1.5	43	33	22
2	0.2	37	39	24
6		14	44	42
16		12	48	40

tion of these spectra were found using 3–4 peaks (see Figure 6) which could be assigned to  $\alpha$ ,  $\beta$ , and  $\gamma$  carbons. It is evident from Figures 5 and 6 and Table 3B that the extent of carburization in terms of total equivalent carbon monolayers increases with increasing pretreatment duration in CO; quantitatively, the equivalent carbon monolayers are 6.6, 13.1, 20.8, and 21.2 layers after 1, 2, 6, and 16 h, respectively. The amount of C<sub>α</sub> is initially very small, decreases after 2 h, and completely disappears after 6 h of pretreatment. Table 3C shows that fractional compositions for the  $\beta$  carbon is initially large and decreases with time; at the same time, total carbides ( $\gamma_1$  and  $\gamma_2$ ) steadily increase with pretreatment time, from 3.7 monolayers (1 h) to 18.6 monolayers (16 h). Thus, carbides ( $\gamma_1$ ,  $\gamma_2$ ) dominate after 6 h; moreover,  $\gamma_1$  is apparently partially converted to  $\gamma_2$  over time. It should be emphasized that during pretreatment for up to 16 h in CO, no graphitic carbon is observed.



**Figure 8.** TPH spectra of 10 wt % Fe/1% Pt/0.2% K/SiO<sub>2</sub> after pretreatment in syngas ( $H_2/CO = 1.0$ ) at 280 °C for 1, 2, 6, and 16 h, respectively.



**Figure 9.** TPH spectra of 10 wt % Fe/1% Pt/0.2% K/SiO<sub>2</sub> after pretreatment in syngas ( $H_2/CO = 1.0$ ) at 280 °C for 16 h and reaction ( $T = 265$  °C,  $P = 10$  atm in  $H_2/CO = 1.0$ ) for 150 h (wax intact and removed), respectively.

Trends observed for carbon species transformations with pretreatment time in FePtK/SiO<sub>2</sub> pretreated in  $H_2/CO$  at 280 °C (Figure 8) are qualitatively similar to those for CO pretreatment; i.e., an upward shift in carbon species peak temperature and increasing peak intensity with increasing pretreatment time are observed. However, peak maxima are shifted to significantly higher temperatures for each pretreatment period; moreover, following pretreatment for 16 h, a substantial fraction of the peak area is in the range of 700–760 °C, indicating a significant quantity of graphitic carbon to be present. The fraction of  $\beta$  carbon is also corresponding less.

Figure 9 shows two TPH spectra collected on a spent FePtK catalyst after pretreatment in syngas ( $H_2/CO = 1.0$ ) for 16 and 150 h of reaction at 265 °C and 10 atm. The wax in one of the catalyst samples was kept intact while it was removed by Soxhlet extraction (in air) from the other. A dramatic effect of the Soxhlet wax extraction on carbonaceous species is observed by (1) loss of carbonaceous material (<550 °C) and (2) a decrease in the intensities of the iron carbide peaks (600–700 °C) with a simultaneous shift to much higher temperature (750 °C).

(2) *Isothermal Transient Measurement (ITM) of Catalyst Selectivity.* Isothermal transient FTS rate measurements ( $H_2/$

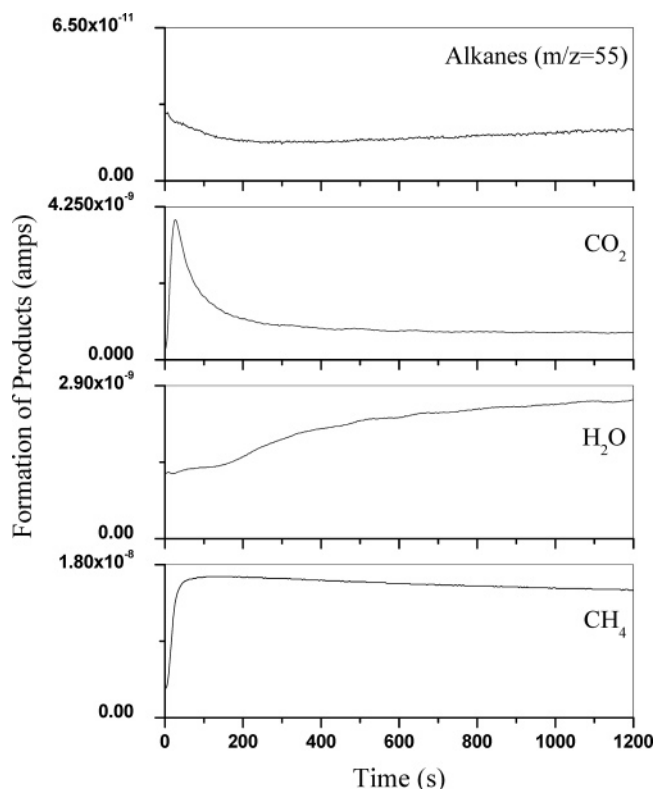


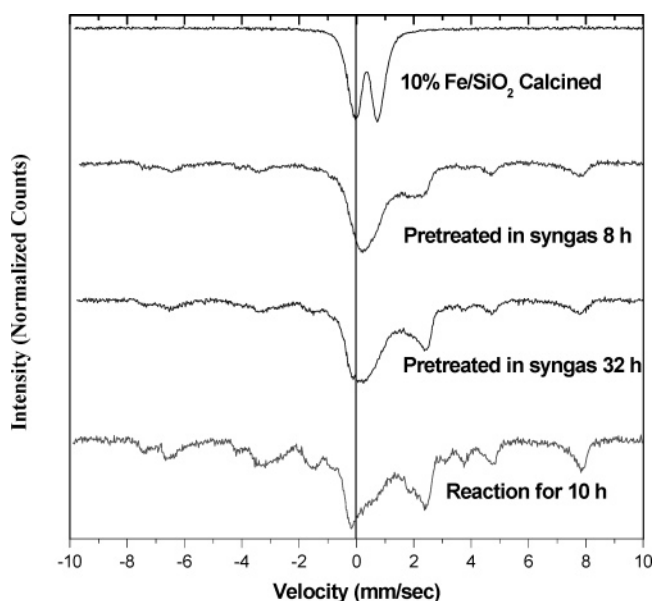
**Figure 10.** Rate of formation of  $CH_4$ ,  $H_2O$ ,  $CO_2$ , and alkanes ( $m/z = 55$ ) as a function of time during contact with synthesis gas at 265 °C for 10 wt % Fe/1% Pt/0.2% K/SiO<sub>2</sub> ( $T = 265$  °C,  $P = 10$  atm in  $H_2/CO = 1.0$ ) after pretreatment in  $H_2/CO = 1.0$  at 280 °C.

$CO = 1.0$ ,  $P = atm$ , 280 °C) were carried out using on-line mass spectrometric analysis following pretreatment of FePtK/SiO<sub>2</sub> in  $H_2$ ,  $H_2/CO$ , or  $CO$ . Representative isothermal transients showing evolution of several FTS products ( $CH_4$ ,  $H_2O$ ,  $CO_2$ , and alkanes collected with an  $m/z = 55$ ) are plotted as a function of time in Figure 10 after pretreatment in  $H_2/CO = 1.0$ . The rate of  $CH_4$  formation was used as a measure of FTS rate since under these conditions methane is the principal product.

The simultaneous formation of  $CH_4$ ,  $H_2O$ ,  $CO_2$ , and alkanes is apparent during the first 100 s of FTS after pretreatment in  $H_2/CO$  (see Figure 10); the same behavior was evident for samples pretreated in  $CO$  or  $H_2$ . Following pretreatment in  $H_2/CO$ , the rate of  $CH_4$  formation (hence FTS rate) increases sharply, reaching a maximum during the initial 100 s of contact with syngas, after which it decreases very slowly with time (Figure 10). This behavior was essentially the same for the other two pretreatments. The alkane concentration for the  $H_2/CO$ -pretreated catalyst (Figure 10) decreases at the beginning and then levels off after 200 s. By comparison the alkane product concentration for the  $H_2$ -pretreated catalyst (not shown) initially increased followed by a fairly rapid decrease after 100 s, while the alkane concentration during reaction on the  $CO$ -pretreated catalyst steadily increased rapidly to 300 s, after which it increased very slowly. The rate of  $CO_2$  formation for the  $H_2/CO$ -pretreated catalyst quickly reaches a maximum in less than 30 s and then drops first rapidly and then slowly (Figure 10); the  $CO_2$  transient after  $H_2$  pretreatment was qualitatively similar, although the peak height was smaller, while that for the  $CO$ -pretreated catalyst quickly increased to a steady value. After  $H_2$  pretreatment water formation rate increased through a maximum at 30 s while that after  $H_2/CO$  pretreatment steadily increased (Figure 10); the  $H_2O$  transient after  $CO$  pretreatment rose sharply in 200 s to a steady value. It is significant that, for

**TABLE 4: CO Chemisorption Uptake after 1 h of Pretreatment in 20% CO/He (Compared with H<sub>2</sub> Chemisorption and BET Surface Area Measurements)**

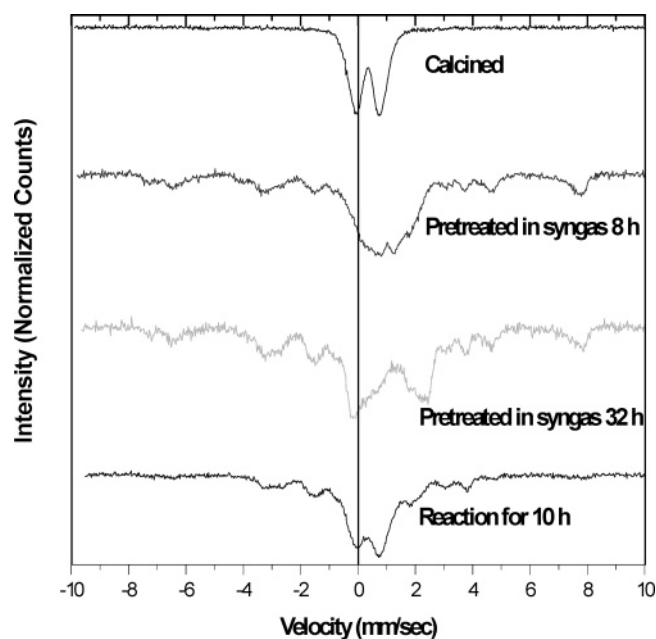
catalyst	Fe/SiO <sub>2</sub>	FePt/SiO <sub>2</sub>	FePtK/SiO <sub>2</sub>
CO <sub>x</sub> desorbed before RT CO chemisorption μmol/g catalyst (mmol/g-atom Fe)	1.1 (0.68)	2.83 (1.7)	50.1 (30)
CO <sub>x</sub> desorbed after RT CO chemisorption μmol/g catalyst (mmol/g-atom Fe)	1.2 (0.72)	74.1 (45.0)	276.6 (167)
CO irreversibly chemisorbed μmol/g-catalyst (mmol/g-atom Fe)	0.1 (0.04)	71.3 (43.3)	226.5 (137)
H <sub>2</sub> uptake μmol/g-catalyst	44.5	51.1	56.5
BET SA m <sup>2</sup> /g calcined catalyst	242	266	296

**Figure 11.** In situ Mössbauer spectra of 10 wt % Fe/SiO<sub>2</sub> after pretreatments and reaction in H<sub>2</sub>/CO = 1.0, 10 atm, total flow = 2 NL/gcat-h (spectra collected at 298 K).

all pretreatments, significant quantities of methane, C<sub>2</sub>+ alkanes, and other products are produced almost immediately.

(3) *TPD Measurements of CO Adsorption Site Density.* CO active site density measurements were carried out on Fe, FePt, and FePtK catalysts using the method of Li et al.<sup>1,37</sup> Two sequential temperature-programmed desorption (TPD) runs were performed (for details see Experimental Section). The quantity desorbed in the first run is total CO<sub>x</sub> after CO chemisorption on a surface conditioned under reaction, while that desorbed during the second run is probably produced from secondary surface reaction, that is, reaction of iron carbides (FeC<sub>x</sub>) and strongly adsorbed carbon species with unreduced neighboring Fe oxides.<sup>1</sup> The difference in peak area under these two sets of TPD spectra is taken as a measure of active sites available for irreversible CO chemisorption under FTS conditions. The CO chemisorption uptakes for these two steps, previously measured H<sub>2</sub> chemisorption uptakes, and BET surface area are compared in Table 4.

It is apparent from Table 4 that Pt and PtK promoters dramatically increase the number of sites that strongly adsorb CO; i.e., the strongly chemisorbed CO uptake for unpromoted Fe/SiO<sub>2</sub> is only 0.1 μmol/g-catalyst, while for Pt- and PtK-promoted catalysts, irreversible CO uptakes are 71.3 to 226.5, respectively. The overall trend of promoter effects on CO chemisorption is in qualitative agreement with the H<sub>2</sub> chemisorption result; i.e., H<sub>2</sub> uptake increases from 44.5 μmol/g for Fe/SiO<sub>2</sub> to 51.1 and 56.5 μmol/g respectively for Pt- and PtK-

**Figure 12.** In situ Mössbauer spectra of 10 wt % Fe/1% Pt/0.2% K/SiO<sub>2</sub> after pretreatments and reaction in H<sub>2</sub>/CO = 1.0, 10 atm, total flow = 2 NL/gcat-h (spectra collected at 298 K).

promoted catalyst, although the relative changes are quantitatively much less dramatic for H<sub>2</sub> relative to CO.

**High-Pressure in Situ Mössbauer Studies.** High-pressure in situ Mössbauer absorption spectroscopy (MAbs) was used to follow the iron phase transformations under realistic FTS conditions, namely, 10 atm and 265 °C. MAbs allows quantitative identification of iron phases in iron-containing catalysts following or during treatment in controlled gaseous environments.<sup>42</sup> Spectra for Fe and FePtK catalysts are shown in the Figures 11 and 12, respectively. Compositional changes in terms of percent peak area of the different iron species for these two catalysts during a series of in situ pretreatments and reactions are listed in Table 5. Average values of Mössbauer parameters associated with various iron species are shown in Table 6.

As shown in Figures 11 and 12 and their corresponding tables, spectra for both calcined Fe and FePtK initially consist of a nearly symmetric quadrupole doublet of broad lines characteristic of highly dispersed Fe<sub>2</sub>O<sub>3</sub>. After a brief exposure to a syngas pretreatment environment (H<sub>2</sub>/CO = 1.0), these superparamagnetic (SP) Fe<sub>2</sub>O<sub>3</sub> nanoparticles are quickly reduced to Fe<sub>3</sub>O<sub>4</sub> of different particle sizes [ferromagnetic (FM) and SP] and ferrous ions (Fe<sup>2+</sup>). Due to the difficulties in detecting SP-supported iron species in the absence of applied magnetic fields, the coexistence of SP Fe<sub>3</sub>O<sub>4</sub> and/or Fe carbides (Fe<sub>2</sub>C and Fe<sub>5</sub>C<sub>2</sub>) on the iron/silica catalysts cannot be ruled out. No FM metallic iron was detected. Nevertheless, SP iron cannot be ruled out either.



**TABLE 5: Phase Transformations of 10% Fe/SiO<sub>2</sub> and 10% Fe/1% Pt/0.2 % K/SiO<sub>2</sub> from High Pressure in Situ Mössbauer Spectroscopy (FTS at 265 °C, 10 atm)**

	iron species (% area)				
	Fe <sub>2</sub> O <sub>3</sub> (sp)	Fe <sub>3</sub> O <sub>4</sub> or Fe <sub>2.5</sub> C (sp)	Fe <sub>3</sub> O <sub>4</sub> (FiM)	Fe <sub>2.5</sub> C	Fe <sup>2+</sup>
<i>10% Fe/SiO<sub>2</sub></i>					
calcined	100				
pretreated in H <sub>2</sub> /CO = 1.0 for 8 h		66.8	20.6		12.6
pretreated in H <sub>2</sub> /CO = 1.0 for 32 h		55.4	18.7	8.5	17.5
synthesis for 10 h		23.0	25.9	27.0	24.2
<i>10% Fe/1% Pt/0.2% K/SiO<sub>2</sub></i>					
calcined	100				
pretreated in H <sub>2</sub> /CO = 1.0 for 8 h		40.8	24.0	19.0	16.2
pretreated in H <sub>2</sub> /CO = 1.0 for 32 h		26.2	19.9	34.5	19.4
synthesis for 10 h		57.4	5.1	30.2	4.3

**TABLE 6: Mössbauer Spectroscopy Parameters of 10% Fe/SiO<sub>2</sub> and 10 wt % Fe/1% Pt/0.2% K/SiO<sub>2</sub> during in Situ<sup>a</sup> Reaction (Spectra Collected at 298 K for 24 h)**

iron phase	iron site	IS <sup>b</sup> (mm/s)	ΔE <sub>Q</sub> <sup>c</sup> (mm/s)	HFS (KOe)
<i>10 wt % Fe/SiO<sub>2</sub></i>				
Fe <sub>2</sub> O <sub>3</sub> (sp)		0.35	1.07	
		0.35	0.63	
Fe <sub>3</sub> O <sub>4</sub> (FiM <sup>d</sup> )	A	0.28 ± 0.02	−0.04	471
	B	0.62 ± 0.01	−0.05	437
χ-Fe <sub>2.5</sub> C (295 K)	I	0.31 ± 0.02	0.15	186
	II	0.18 ± 0.09	0.09	221
	III	0.27 ± 0.10	0.18	115
Fe <sup>2+</sup> (295 K)		1.30 ± 0.02	2.17 ± 0.09	
Fe <sub>3</sub> O <sub>4</sub> (sp) or Fe <sub>2.5</sub> C (sp) <sup>e</sup>		0.28 ± 0.08	0.67 ± 0.06	
		0.43 ± 0.15	1.12 ± 0.07	
<i>10 wt % Fe/1% Pt/0.2% K/SiO<sub>2</sub></i>				
Fe <sub>2</sub> O <sub>3</sub> (sp)				
Fe <sub>3</sub> O <sub>4</sub> (FiM <sup>d</sup> )	A	0.20 ± 0.07	−0.04	460
	B	0.62 ± 0.03	0.03	438
χ-Fe <sub>2.5</sub> C (295 K)	I	0.21 ± 0.05	0.01	179
	II	0.32 ± 0.06	−0.03	214
	III	0.26 ± 0.01	0.06	111
Fe <sup>2+</sup> (295 K)				
		1.09 ± 0.16	1.78	
Fe <sub>3</sub> O <sub>4</sub> (sp) or Fe <sub>2.5</sub> C (sp) <sup>e</sup>		0.37 ± 0.03	0.87 ± 0.28	
		0.59 ± 0.15	0.82	

<sup>a</sup> In situ treatment was conducted at 1 atm; gas largely bypassed the sample, possibly leading to incomplete carbide formation. <sup>b</sup> Relative to α-Fe. <sup>c</sup> For magnetically split spectra this value is 2ε', ΔE<sub>Q</sub> = 2ε' if φ = 0. <sup>d</sup> Ferrimagnetic Fe<sub>3</sub>O<sub>4</sub>. <sup>e</sup> Superparamagnetic Fe<sub>3</sub>O<sub>4</sub> or Fe<sub>2.5</sub>C.

After an 8 h pretreatment of the calcined, unpromoted Fe/silica, Fe<sub>2</sub>O<sub>3</sub> is reduced to a mixture of Fe<sub>3</sub>O<sub>4</sub> and Fe<sup>2+</sup> as shown in Figure 11. The observed quadrupole splitting and the corresponding Mössbauer parameters for Fe<sup>2+</sup> in both catalysts (IS = 1.30, QS = 2.17) are characteristic of high-spin ferrous ions in oxides, indicative of partial reduction to the ferrous state during syngas pretreatment and reaction. The broad line widths and intensity differences in the absorption peaks associated with Fe<sup>2+</sup> species indicate that different iron environments are present. No FM carbide formation is observed for the Fe catalyst after 8 h of exposure to syngas at 280 °C. In contrast, a significant quantity (19.0%) of FM Hägg carbide (also called χ-carbide; stoichiometry of Fe<sub>2.5</sub>C) can be found in the FePtK/silica catalyst after similar pretreatment. While two carbides (ε' and χ) were identified in TPH experiments, only χ-carbide was observed by Mössbauer spectroscopy—apparently the spectra for the two carbides of very similar composition are highly overlapped and cannot be discriminated given the broad lines, although the broad peaks are consistent with iron in two or more carbide environments.

Following additional 24 h pretreatments in CO/H<sub>2</sub> ferromagnetic carbide content was observed to increase to 8.5% and 34.5% for Fe/silica and FePtK/silica catalysts, respectively (Table 5). The ferromagnetic (FM) carbide content for Fe/silica

increases further to 27% after an additional 10 h of synthesis, while that of the FePtK catalyst apparently decreases slightly to 30.2%. However, because SP Fe<sub>3</sub>O<sub>4</sub> and Fe<sub>2.5</sub>C cannot be resolved using room-temperature MAbS (in the absence of an external magnetic field), it is possible that they coexist on the surface of catalyst. Moreover, it is conceivable that some of the FM Fe<sub>2.5</sub>C is converted during reaction to SP Fe<sub>2.5</sub>C, and thus the total amount of Fe<sub>2.5</sub>C (FM and SP) might remain constant or increase for the FePtK catalyst. Indeed, while the total amount of SP Fe<sub>3</sub>O<sub>4</sub> and Fe<sub>2.5</sub>C in the Fe catalyst decreases from 66.8% to 23.0% during pretreatment and reaction, the total amount of SP phases in the FePtK catalyst initially decreases from 40.8% to 26.2 during pretreatment and then increases to 57.4% during reaction. Significantly, more ferrous iron (24.2%) is present in the unpromoted iron catalyst after pretreatment and 10 h of synthesis compared to only 4.3% for the Pt/K promoted catalyst.

These observations reveal significant changes in phase composition and nanostructure during pretreatment and reaction with trends to the formation of reduced nanophases, i.e., Fe-(II), Fe<sub>3</sub>O<sub>4</sub>, Hägg carbide. The addition of Pt and K promoters contributes to more rapid and extensive reduction while favoring conversion to highly dispersed phases. The addition of platinum causes a marked increase in the fractions of SP Fe<sub>3</sub>O<sub>4</sub> and Fe<sub>2.5</sub>C



following syngas pretreatments (Table 5). Platinum appears to be present in a separate phase from iron, as no significant amount of PtFe alloy formation was detected.

#### 4. Discussion

**Carbon Phase Transformations during Pretreatment and Reaction.** (1) *Effects of Pretreatment Gas and Promoter.* Effects of pretreatment gas on surface carbon phase transformation were systematically studied in this work. Following exposure to H<sub>2</sub>, H<sub>2</sub>/CO, and CO gases as a function of time or followed by reaction, marked differences in catalyst surface carbon species as revealed by TPH are evident for the Fe/silica and FePtK/silica catalysts. For example, in the case of FePtK/silica peak temperature and therewith the fraction of inactive, graphitic carbon increase in the order of pretreatment with H<sub>2</sub>, CO, and H<sub>2</sub>/CO, while the quantity of reactive, atomic surface carbon (C<sub>α</sub>) and the ratio C<sub>α</sub>/C<sub>β</sub> increases with increasing H<sub>2</sub> content in pretreatment gas. This suggests that adsorbed H<sub>2</sub> plays multiple roles in the complex transformations of carbon species observed on iron surfaces; i.e., during pretreatment and reaction H<sub>2</sub> favors the formation of reactive, atomic carbon at the expense of C<sub>β</sub>; by contrast, the near or complete absence of C<sub>α</sub> and the larger quantity of C<sub>β2</sub> (polymeric carbon) following pretreatment in CO (Table 3B) implies that C<sub>α</sub> is apparently converted more readily to C<sub>β2</sub> in the absence of hydrogen. However, the presence of both H<sub>2</sub> and CO during pretreatment appears to accelerate transformations of C<sub>α</sub> to C<sub>β1</sub> (polymethylene) and of C<sub>β1</sub> to C<sub>δ</sub> (graphitic carbon).

In isothermal transient measurements, formation of CH<sub>4</sub>, H<sub>2</sub>O, CO<sub>2</sub>, and alkanes (*m/z* = 55) was observed within seconds of initial contact with reactant H<sub>2</sub>/CO at 265 °C, following pretreatment in each of three atmospheres (i.e., H<sub>2</sub>, H<sub>2</sub>/CO, or CO). Thus, it appears that irrespective of pretreatment and surface species distribution, active sites are formed almost instantaneously through modifications of the surface carbon and iron chemistries and reach a semi-steady state within minutes. The isothermal transient measurements of this study are consistent with those of Li et al.<sup>1</sup> who concluded that the formation of active sites required for FTS on unsupported iron is rapid on either carbided or oxidized iron surfaces; i.e., CH<sub>4</sub> formation rate reaches a semi-steady state in less than 100 s for either starting material.

Nevertheless, it should be emphasized that true steady-state activity (and selectivity) of iron catalysts is not reached in minutes but rather over periods of several hundred hours (see Figure 1). Moreover, as demonstrated in Figure 1, the approach to steady state is markedly different for different pretreatment conditions. Based on the results of our pretreatment studies discussed above, we conclude that the observed differences in activity-time behavior over tens of hours are due to differences in the distributions of carbonaceous and iron species on the surface of Fe/silica, originally determined by pretreatment atmosphere (and temperature), further affected by continuing changes in the distribution of surface species during reaction and affected continually during both pretreatment and reaction by promoter level. It also follows that long-term deactivation behavior is likely to be influenced by the pretreatment atmosphere since pretreatment conditions (gas and temperature) determine the early distribution of inactive beta and graphitic carbons on the surface; e.g., fractions of beta and graphitic carbons are higher for H<sub>2</sub>/CO pretreatment relative to H<sub>2</sub> pretreatment.

While the result of this and previous studies provide a definitive picture of transformations of surface and bulk

carbonaceous species and bulk iron species during pretreatment and reaction on iron FT catalysts, the chemistry of surface iron species and active sites in FTS remains largely a mystery.

(2) *Effects of Pretreatment Time.* Effects of pretreatment duration on carbon species distribution in FePtK/silica are qualitatively similar for CO or H<sub>2</sub>/CO environments. Progressive carburization of the surface and bulk of supported iron is evident from Figures 5–8 and Table 3B. For example, following only 1 h of pretreatment in 20%CO/He the carbon inventory consists of 2.9 monolayer (ML) equivalents of surface carbon (0.10 and 2.8 ML of C<sub>α</sub> and C<sub>β</sub>) and 3.7 ML equivalents of bulk iron carbides (2.2 and 1.5 ML of γ<sub>1</sub> and γ<sub>2</sub>) for a total of 6.6 ML. But after 16 h of CO pretreatment (same conditions), the total carbon inventory has grown to 21.3 ML, of which 2.7 ML is surface carbon (C<sub>β</sub>) and 18.6 ML is bulk carbides. Following a 16 h pretreatment in CO and 10 h of reaction, the overall carbon inventory of 20.9 ML equivalents is essentially the same as following the 16 h pretreatment (see Table 2B), although the distribution of surface and bulk carbon species following pretreatment and reaction is significantly different; it includes, for example, more surface carbon and less bulk carbides, i.e., 4.3 ML of surface carbons (C<sub>α</sub>, C<sub>β</sub>, and C<sub>δ</sub>) and 16.6 ML equivalents of bulk carbide (C<sub>γ</sub>). The presence in pretreated or working iron catalysts of 2–6 monolayer equivalents of surface carbon or condensed hydrocarbons (e.g., polymeric methylene or C<sub>β</sub>) observed in this study is consistent with observations in previous studies<sup>16,31–33</sup> of multilayer equivalents of hydrocarbonaceous material on the surface following reaction, consistent with a model of a working iron catalyst surface buried beneath several layers or a film of porous, carbonaceous material.<sup>31</sup>

(3) *Effects of Wax Extraction.* The effects of oxidation/passivation on carbide species are evident from the comparison in Figure 9. Relative to the spent FePtK/SiO<sub>2</sub> catalyst containing wax, the loss of low-temperature carbonaceous peaks due to Soxhlet wax extraction is expected; however, the disappearance of carbide peaks and appearance of a higher temperature peak indicative of highly graphitic carbon are somewhat unexpected. Nevertheless, Shroff and Datye<sup>43</sup> observed that the active iron carbide phase was partly oxidized upon exposure to air during handling of a spent iron catalyst consistent with the results of this work. Both observations (Shroff and Datye's and that of this study) can be explained by progressive oxidation of carbide nodules during air exposure, passivation, or a conventional Soxhlet wax extraction in air.

**Activity-Structure Correlations.** (1) *CO Site Density and Catalytic Activity.* Direct measurement of catalytic site density for iron FT catalysts has been said to be impossible due to the chemical complexity of the active surface which may contain iron oxides, carbides, and metal.<sup>44</sup> Nevertheless, Li et al.<sup>1</sup> have claimed a new method of determining active site density of unsupported iron catalysts involving measurement of irreversibly chemisorbed CO. The applicability of this method to measurement of active sites on silica-supported iron catalysts was examined in this study.

It is well-known that during adsorption and/or reaction both single-bonded (linear) and bridge-bonded CO species are observed on iron and platinum surfaces.<sup>45</sup> Single-bridged CO species are more strongly adsorbed than linear CO species. CO typically dissociates to carbon and oxygen atoms on iron surfaces at temperatures above about 150 °C, while at room temperature it adsorbs in the molecular form only. Thus, dissociated and molecular forms of carbon monoxide probably coexist on the carbon-covered iron oxide/metal/carbide surface during and following reaction.<sup>46</sup> Furthermore, FT reaction could

take place on sites that adsorb CO either reversibly or irreversibly. This conclusion is supported by the results of this and our previous study,<sup>24</sup> showing that the Fe/SiO<sub>2</sub> catalyst with an uptake only 0.1  $\mu\text{mol/g}$  of irreversibly chemisorbed CO is nevertheless quite active.<sup>47</sup> Thus, the method proposed by Li et al.<sup>1</sup> to measure irreversibly chemisorbed CO does not provide a quantitative measure of active sites on silica-supported iron. The net result of using Pt and K promoters is higher BET and metal surface areas (see Table 4) and thus significantly higher uptakes of CO<sub>irrev</sub>. Indeed, the CO<sub>irrev</sub> site density for iron catalysts of this study increases in the order (Table 4) Fe/SiO<sub>2</sub>, FePt/SiO<sub>2</sub>, and FePtK/SiO<sub>2</sub> in qualitative agreement with the trends for increasing total H<sub>2</sub> chemisorption uptake and catalytic activity of these catalysts from our previous study.<sup>24</sup> Thus, while CO<sub>irrev</sub> site density reflects a trend in catalytic activity, it is apparently only a qualitative measure of catalytic performance.

(2) *Surface Carbon Reactivity and Initial Catalytic Activity.* The pretreatment environment has been reported to significantly influence initial catalytic activity.<sup>12,47</sup> For example, it was observed that a precipitated iron catalyst (100 Fe/3 Cu/16 SiO<sub>2</sub>) pretreated in H<sub>2</sub> was more active and reached steady state more rapidly than the corresponding catalyst treated in CO;<sup>12</sup> the syngas pretreated catalyst was intermediate in terms of both initial activity and time to reach steady state. Based on the isothermal transient studies of the present work and the previous study of Li et al.,<sup>1,40</sup> it may be surmised that carburization of Fe<sub>3</sub>O<sub>4</sub> clusters starts from the conversion of their near-surface layers to form FeC<sub>x</sub> to quickly provide active sites for FTS. As observed in previous TEM studies, e.g.,<sup>16</sup> the dynamic “thin rim” of surface iron carbide (FeC<sub>x</sub>) nodules develops independently of the composition of underlying “kernel” which may be a mixture of rapidly interconverting iron carbides and oxides. Since FTS rate increases dramatically during the initial stages of carburization, the formation of these active carbide nodules is probably an important factor in determining the initial and steady-state catalyst activities. The synergistic effects of K and Pt in our FePtK catalyst are manifest in faster rates of carburization and formation of well-dispersed carbides, consistent with the previous studies of Li et al.<sup>1,40</sup> These small iron carbide clusters apparently provide abundant CO chemisorption sites for the FePtK catalyst, explaining the higher BET surface area, higher CO<sub>irrev</sub> uptake, and H<sub>2</sub> uptake observed for FePtK compared to FePt and Fe catalysts (Table 4).

The initial FTS activity observed for the FePtK catalyst varies greatly with pretreatment atmosphere, decreasing in the following order of pretreatment gas: H<sub>2</sub>, H<sub>2</sub>/CO, and CO (see Figure 1). Based on TPH data from Table 2, C <sub>$\alpha$</sub>  coverage decreases in the same order of pretreatment gas, i.e., H<sub>2</sub> pretreated (1.1 monolayers) > H<sub>2</sub>/CO (0.8 monolayers) > CO pretreated (0.3 monolayers) pretreated. Thus, a correlation of initial catalytic activity with C <sub>$\alpha$</sub>  coverage is apparent (Figure 13). A similar correlation was reported by Lee and Bartholomew<sup>23</sup> for supported cobalt catalysts, that is, a linear correlation was found between initial CH<sub>4</sub> turnover frequency in CO hydrogenation with the relative area of C <sub>$\alpha$</sub>  coverage measured after CO dissociation at 250 °C.

**Toward More Comprehensive Models of Iron and Carbon Transformations in FTS.** Bulk and surface changes in the speciation of iron during pretreatment of and FTS reaction on unsupported iron catalysts have been well-studied using in situ Mössbauer spectroscopy,<sup>35,48</sup> XRD,<sup>6,49–51</sup> TEM,<sup>16,52</sup> and TPH/TPO<sup>25,27,32</sup>. Sequential bulk phase modifications during the activation process from Fe<sub>2</sub>O<sub>3</sub> to Fe<sub>3</sub>O<sub>4</sub> to FeC<sub>x</sub> (iron carbides) have been reported.<sup>16,40</sup> The same sequence of transformations

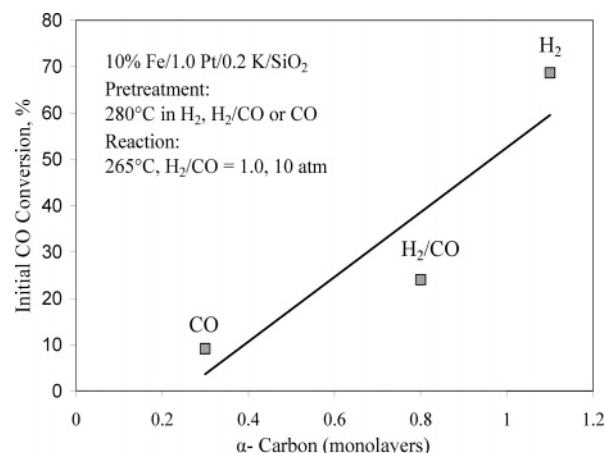


**Figure 13.** Correlation between  $\alpha$ -carbon content and initial catalytic activity (CO conversion %).

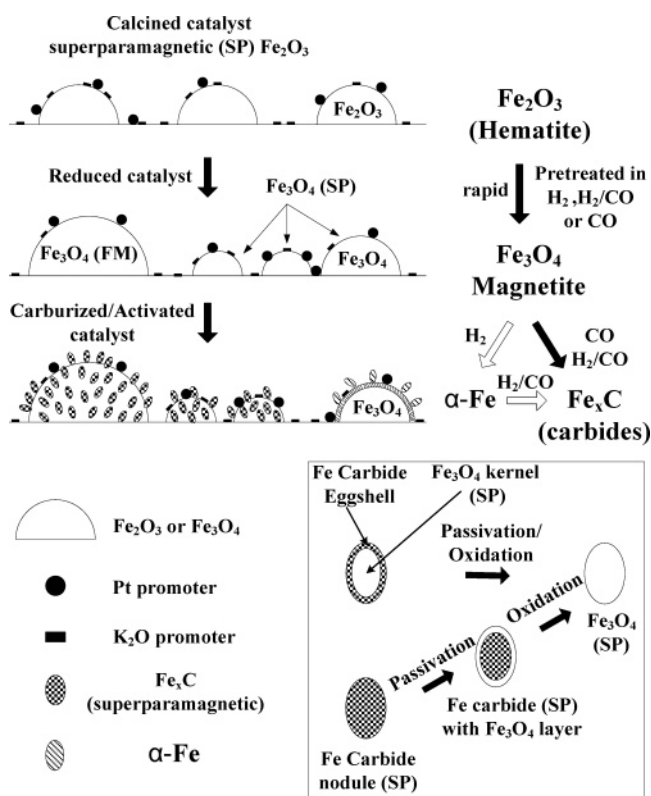


**Figure 14.** Schematic of nanocarbide nodule model for iron phase transformations.

for iron phases are observed in this study for silica-supported iron catalysts. Surface transformations of carbon-containing species on unsupported and supported iron can be inferred from this study and recent transient kinetic and TPH studies<sup>1,33,50</sup> Combining the information from the recent studies with earlier work provides new perspectives that can be incorporated into expanded models of iron and carbon surface and bulk species transformations during pretreatment and FTS reaction; these models address somewhat the roles of promoters and are general for supported and unsupported materials (see Figures 14 and 15).

Figure 14 traces iron phase transformations of a supported iron catalyst promoted with K and Pt from the calcined catalyst through pretreatments in H<sub>2</sub>, CO, or H<sub>2</sub>/CO; it also addresses changes that occur in passivation and air/steam exposure. During pretreatment in either H<sub>2</sub>, CO, or H<sub>2</sub>/CO highly dispersed, superparamagnetic (SP) Fe<sub>2</sub>O<sub>3</sub> undergoes fast reduction to small

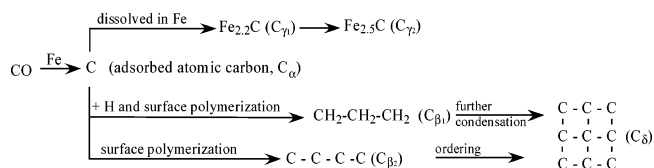


**Figure 15.** Surface and bulk carbon species present in unsupported and supported iron FTS catalysts following pretreatment and reaction.

and large crystallites of  $\text{Fe}_3\text{O}_4$  [SP and ferromagnetic (FM)] as confirmed by the data of this study for unpromoted and promoted iron catalysts. Nevertheless, rates of reduction of  $\text{Fe}_3\text{O}_4$  to iron metal or iron carbides (second step in Figure 14) are significantly lower and the conversion is less extensive for unpromoted relative to K- and/or Pt-promoted Fe/silica catalysts.

For example, following pretreatment for 8 h in  $\text{H}_2/\text{CO}$  of unpromoted Fe/silica,  $\text{Fe}_2\text{O}_3$  was reduced to  $\text{Fe}^{2+}$  interacting strongly with the support and a mixture of large ferromagnetic and highly dispersed, superparamagnetic crystallites of  $\text{Fe}_3\text{O}_4$  (see Table 5). The presence of ferrous ions and the absence of iron carbide are indicative of slow, incomplete reduction of the iron. By contrast, the reduction of FePtK/silica after 8 h is much more rapid and complete as shown by extensive carbide formation (Table 5). Moreover, after 32 h of pretreatment and 10 h of synthesis, the percentage of  $\text{Fe}^{2+}$  in FePtK/silica is only 4.3% compared to 24.2% for Fe/silica. The higher rate of reduction and carbide formation in FePtK/silica can be attributed to the presence of small Pt clusters on the surface of  $\text{Fe}_3\text{O}_4$  crystallites (Figure 14) formed early in the reduction and which dissociatively adsorb  $\text{H}_2$ , producing atomic hydrogen that spills over to the surface of  $\text{Fe}_3\text{O}_4$  crystallites, reducing surface oxides to Fe metal. Surface Fe in turn dissociates CO to form highly dispersed carbide nodules, leading to an increase in active and BET surface areas. As the carburization process continues, the layer of carbide nodules surrounding the  $\text{Fe}_3\text{O}_4$  core increases in thickness following either a nucleation mechanism or a shrinking core model until (in the case of small crystallites) the entire crystallite is carburized. The rapid rise in activity of  $\text{H}_2$ -pretreated FePtK/SiO<sub>2</sub> during the first 2–3 h of reaction may be due to rapid carburizing of small iron clusters generated during mild  $\text{H}_2$  reduction, following which activity is relatively constant.

Results of the present and previous studies show that the conversion of  $\text{Fe}_3\text{O}_4$  to iron carbides is dynamic and reversible depending upon the environment.<sup>1</sup> Under oxidizing conditions (e.g., at high water and  $\text{CO}_2$  partial pressures), layers of surface  $\text{Fe}_3\text{O}_4$  can form on an iron carbide kernel; ultimately pure magnetite particles could be formed. Since the highly dispersed carbide nodules or layers may have diameters or thicknesses smaller than 3–10 nm, they can be difficult to observe by either XRD or Mössbauer spectroscopy—in the latter case because they are superparamagnetic even at room temperature. Because of relaxation effects, the Mössbauer spectrum of a superparamagnetic material such as a carbide collapses to a simple doublet that is difficult or impossible to differentiate from that for other oxides or carbides in zero-magnetic field Mössbauer spectroscopy.<sup>53</sup>

The proposed model in Figure 14 could resolve some of the discrepancies regarding the active phase for iron FTS catalysts. For example, Reymond and Teichner<sup>54</sup> proposed that the active phase in FTS is  $\text{Fe}_3\text{O}_4$  since, upon exposure to syngas, their starting material,  $\text{Fe}_3\text{O}_4$ , appeared to be immediately active and did not appear to have changed chemically after reaction based on Mössbauer analysis; however, if highly dispersed iron carbide had been formed during reaction, it would have been oxidized

back to  $\text{Fe}_3\text{O}_4$  during sample transfer in air from the reactor to the spectrometer. Similarly, the single magnetite phase observed by Huang et al.<sup>55</sup> by XRD for their catalyst at peak activity could be explained by (1) oxidation of carbide nodules upon exposure to air and/or (2) the inability of XRD to detect amorphous, thin layers of well-dispersed Fe carbide. In our companion paper,<sup>24</sup> an unexpected lack of correlation between iron carbide ( $\text{Fe}_{2.5}\text{C}$ ) content for spent, air-exposed samples and catalyst activity was found for FePtK/SiO<sub>2</sub>. This observation may be an artifact due to oxidation of highly dispersed iron carbide layers to magnetite particles during transfer of the spent samples in air to our Mössbauer spectrometer.

Figure 15 depicts the formation and transformations of different carbon species observed in previous studies<sup>25–33</sup> on unsupported Fe after reaction at low pressure and in this study on Fe/silica catalysts after reaction at high pressure. Evidence supporting this scheme is discussed and documented in the discussion above. Two additional observations are of note: (1) two forms of beta carbon are observed, i.e., amorphous polymeric carbon formed by CO dissociation in the absence of  $\text{H}_2$  and polymethylene chains or films formed in  $\text{CO}/\text{H}_2$  atmospheres (see Figure 15); (2) the pretreatment-versus-time data of this study are consistent with a series transformation of  $\text{C}_\alpha$  to  $\epsilon'$ -carbide to  $\chi$ -carbide. The  $\epsilon'$ - to  $\chi$ -carbide transformation may occur through precipitation of graphitic carbon.<sup>33,56</sup>

## 5. Conclusions

The pretreatment atmosphere greatly influences activity-time behavior during the first 100 h of reaction. For FePtK/SiO<sub>2</sub>, activity versus time climbs slowly, climbs rapidly, or is fairly constant following pretreatment in CO, syngas ( $\text{H}_2/\text{CO} = 1$ ), or  $\text{H}_2$  respectively. These differences in activity versus time can be explained by differences in the distribution of iron- and carbon-containing surface and bulk species created during pretreatment. Species thus formed include (a) adsorbed, atomic carbon, (b) amorphous, lightly polymerized hydrocarbon or carbon surface species, (c) bulk  $\epsilon'$  and  $\chi$  carbides ( $\text{Fe}_{2.2}\text{C}$  and  $\text{Fe}_{2.5}\text{C}$ ), and (d) disordered and moderately ordered graphitic surface carbons.

Catalytic activity for methane and  $\text{C}_2+$  hydrocarbons is established on unsupported or supported iron within the first few seconds of initiating reaction, following pretreatment in air, CO,  $\text{H}_2$ , or  $\text{H}_2/\text{CO}$  or almost any variety of oxidizing or reducing conditions. Following pretreatment in CO,  $\text{H}_2$ , or  $\text{H}_2/\text{CO}$ , initial catalytic activity is positively correlated with the amount of reactive  $\text{C}_\alpha$  carbon formed on the catalyst surface. However, steady-state activity is typically only reached after several hundred hours of reaction as a result of slow transformations of iron and carbon species at the surface and in the bulk of iron crystallites. Steady-state activity is apparently best correlated with iron carbide surface area.

Based on this and previous studies, a likely scenario of carbon transformations emerges: (a) During pretreatment and reaction, small  $\text{Fe}_2\text{O}_3$  crystallites are rapidly converted to large and small crystallites of  $\text{Fe}_3\text{O}_4$ ; (b) the surfaces of the  $\text{Fe}_3\text{O}_4$  crystallites are relatively slowly reduced to iron metal which dissociates CO to atomic carbon ( $\text{C}_\alpha$ ); (c)  $\text{C}_\alpha$  dissolves into iron to form iron carbides ( $\epsilon'$  and  $\chi$ ) which nucleate into small iron carbide nodules forming layers at the exterior of  $\text{Fe}_3\text{O}_4$  crystallites; (d) carbide layers grow progressively inward at the expense of the  $\text{Fe}_3\text{O}_4$  core; (e) reaction occurs at the surface of each carbide nodule; and (f) during pretreatment and reaction, a portion of the atomic carbon at the surface of each nodule is converted to polymeric forms of amorphous, condensed hydrocarbons ( $\text{C}_\beta$ ) and semicrystalline ( $\text{C}_\delta$ ) carbon.



The addition of Pt and K promoters contributes to more rapid and extensive reduction of  $\text{Fe}_3\text{O}_4$  to highly dispersed iron carbides. Pt effects an increase in the fractions of well-dispersed, superparamagnetic  $\text{Fe}_3\text{O}_4$  and  $\text{Fe}_{2.5}\text{C}$  during syngas pretreatments.

The working FT catalyst probably consists of relatively large  $\text{Fe}_3\text{O}_4$  crystallites, the surfaces of which have been converted to small nodules of  $\epsilon'$  ( $\text{Fe}_{2.0.2}\text{C}$ ) and  $\chi$  ( $\text{Fe}_5\text{C}_2$ ). Nodule surfaces are covered with (a) less than a monolayer of adsorbed, atomic carbon ( $\text{C}_\alpha$ ) of high reactivity, (b) 2–3 monolayer equivalents of amorphous, condensed polymethylene in the form of chains or films ( $\text{C}_\beta$ ) of moderate reactivity, and (c) 2–3 monolayer equivalents of semi-ordered graphitic carbon ( $\text{C}_\delta$ ) films of low reactivity.

Iron carbide nodules, present in a working iron FT catalyst as a well-dispersed phase or as an eggshell layer surrounding large  $\text{Fe}_3\text{O}_4$  particles, are apparently readily oxidized to magnetite ( $\text{Fe}_3\text{O}_4$ ) when exposed to air at room temperature. Soxhlet extraction of a spent iron catalyst removes active carbon forms and oxidized iron carbides to iron oxides, leaving only graphitic carbon on the catalyst surface.

Li et al.'s method of measuring irreversibly chemisorbed CO site density does not provide a quantitative measure of active site density for FTS on silica-supported iron catalyst. It appears that sites for reversibly adsorbed CO may also play a role in the iron-catalyzed Fischer–Tropsch.

**Acknowledgment.** The authors gratefully acknowledge financial support of this work by the U.S. Department of Energy, Division of Fossil Energy, under Contract DE-FG26-98FT40110, Brigham Young University, and the William and Margaret Pope Chemical Engineering Professorship. Collaborations with Professor Abaya K. Datye of the University of New Mexico and Professor Dragomir Bukur of Texas A&M University and their students are likewise gratefully acknowledged. We wish to thank George Huber and Matt Stoker for technical assistance.

## References and Notes

- (1) Li, S.; Ding, W.; Meitzner, G. D.; Iglesia, E. *J. Phys. Chem. B* **2002**, *106*, 85.
- (2) Storch, H. H.; Golumbic, N.; Anderson, R. B. *The Fischer–Tropsch and Related Synthesis*; John Wiley & Sons: New York, 1951.
- (3) Dry, M. E. The Fischer–Tropsch Synthesis. In *Catalysis*; Anderson, J. R., Boudart, M., Eds.; Springer-Verlag: New York, 1981; Vol. 1, p 159.
- (4) Dry, M. E. *J. Mol. Catal.* **1982**, *17*, 133.
- (5) Anderson, R. B. *The Fischer–Tropsch Synthesis*; Academic Press: Orlando, FL, 1984.
- (6) Dictor, R. A.; Bell, A. T. *J. Catal.* **1986**, *97*, 121.
- (7) Soled, S. L.; Iglesia, E.; Fiato, R. A. *Catal. Lett.* **1990**, *7*, 271.
- (8) Rao, K. R. P. M.; Huggins, F. E.; Mahajan, V.; Huffman, G. P.; Rao, V. U. S.; Bhatt, B. L.; Bukur, D. B.; Davis, B. H.; O'Brien, R. J. *Top. Catal.* **1995**, *2*, 71.
- (9) Shroff, M. D.; Kalakkad, D. S.; Coulter, K. E.; Köhler, S. D.; Harrington, M. S.; Jackson, N. B.; Sault, A. G.; Datye, A. K. *J. Catal.* **1995**, *156*, 185.
- (10) Rao, K. R. P. M.; Huggins, F. E.; Huffman, G. P.; Gormley, R. J.; O'Brien, R. J.; Davis, B. H. *Energy Fuels* **1996**, *10*, 546.
- (11) Bukur, D. B.; Lang, X. *Ind. Eng. Chem. Res.* **1999**, *38*, 3270.
- (12) Bukur, D. B.; Lang, X.; Ding, Y. *Appl. Catal., A* **1999**, *186*, 225.
- (13) O'Brien, R. J.; Xu, L.; Bao, S.; Raje, A. P.; Davis, B. H. *Appl. Catal., A* **2000**, *196*, 173.
- (14) Li, S.; Meitzner, G. D.; Iglesia, E. Fischer–Tropsch synthesis catalysts based on Fe oxide precursors modified by Cu and K: structure and site requirements. In *Natural Gas Conversion VI*; Iglesia, E., Spivey, J. J., Fleisch, T. H., Eds.; Studies in Surface Science and Catalysis; Elsevier: Amsterdam, 2001; Vol. 136, p 63.
- (15) Davis, B. H. *Catal. Today* **2003**, *84*, 83.
- (16) Jackson, N. B.; Datye, A. K.; Mansker, L.; O'Brien, R. J.; Davis, B. H. Deactivation and Attrition of Iron Catalysts in Synthesis Gas. In *Studies in Surface Science and Catalysis*; Bartholomew, C. H., Fuentes, G. A., Eds.; Elsevier Science: Amsterdam, 1997; Vol. 111, p 501.
- (17) Zhao, R.; Goodwin, J. G.; Jothimurugesan, K.; Gangwal, S. K.; Spivey, J. J. *Ind. Eng. Chem. Res.* **2001**, *40*, 1320.
- (18) Pham, H. N.; Nowicki, L.; Xu, J.; Datye, A. K.; Bukur, D. B.; Bartholomew, C. H. *Ind. Eng. Chem. Res.* **2003**, *42*, 4001.
- (19) Kalakkad, D. S.; Shroff, M. D.; Köhler, S.; Jackson, N.; Datye, A. K. *Appl. Catal., A* **1995**, *133*, 335.
- (20) Rankin, J. L.; Bartholomew, C. H. *J. Catal.* **1986**, *100*, 533.
- (21) Rameswaran, M.; Bartholomew, C. H. *J. Catal.* **1989**, *117*, 218.
- (22) Bukur, D. B.; Sivaraj, C. *Appl. Catal., A* **2002**, *231*, 201.
- (23) Lee, W. H.; Bartholomew, C. H. *J. Catal.* **1989**, *120*, 256.
- (24) Xu, J.; Bartholomew, C. H.; Sudweeks, J.; Eggett, D. L. *Top. Catal.* **2003**, *26*, 55.
- (25) Ahlafi, H.; Bennett, C. O.; Bianchi, D. *J. Catal.* **1992**, *133*, 83.
- (26) Menon, P. G. Hydrogen as a tool for characterization of catalyst surface by chemisorption, gas titration, and temperature-programmed techniques. In *Hydrogen Effects in Catalysis. Fundamentals and Practical Applications*; Paal, Z., Menon, P. G., Eds.; Marcel Dekker: New York, 1988; p 117.
- (27) Eliason, S. A. Deactivation by Carbon of Unpromoted and Potassium-Promoted Iron Fischer–Tropsch Catalysts. Ph.D., Brigham Young University, Provo, UT, 1994.
- (28) Bartholomew, C. H. *Catal. Rev.—Sci. Eng.* **1982**, *24*, 67.
- (29) McCarty, J. G.; Hou, P. Y.; Sheridan, D.; Wise, H. Reactivity of Surface Carbon on Nickel Catalysts: Temperature-Programmed Surface Reaction with Hydrogen and Water. In *Coke Formation on Metal Surfaces*; Albright, L. F., Baker, R. T. K., Eds.; Maple Press: Washington, DC, 1982; p 253.
- (30) Bowman, R. M.; Bartholomew, C. H. *Appl. Catal.* **1983**, *7*, 179.
- (31) Dwyer, D. J. *Prepr.—Am. Chem. Soc., Div. Pet. Chem.* **1984**, *29*, 715.
- (32) Galuszka, J.; Sano, T.; Sawicki, J. A. *J. Catal.* **1992**, *136*, 96.
- (33) Eliason, S. A.; Bartholomew, C. H. In *Catalyst Deactivation 1997*; Bartholomew, C. H., Fuentes, G. A., Eds.; Studies in Surface Science and Catalysis; Elsevier: Amsterdam, 1997; Vol. 111, p 517.
- (34) Dumesic, J. A.; Topsøe, H. *Adv. Catal.* **26**, 121.
- (35) Bartholomew, C. H.; Boudart, M. *J. Catal.* **1973**, *29*, 278.
- (36) Bianchi, D.; Borcar, S.; Teule-Gay, F.; Bennett, C. O. *J. Catal.* **1983**, *82*, 442.
- (37) Woo, H. S.; Fleisch, T. H.; Foley, H. C.; Uchiyama, S.; Delgass, W. N. *Catal. Lett.* **1990**, *4*, 93.
- (38) Xu, J. Rational Design of Silica-Supported Platinum Promoted Iron Fischer–Tropsch Synthesis Catalysts Based on Activity-Structure Relationships. Ph. D Dissertation, Brigham Young University, Provo, UT, 2003.
- (39) Ozdogan, S. Z.; Gochis, P. D.; Falconer, J. L. *J. Catal.* **1983**, *83*, 257.
- (40) Li, S.; Meitzner, G. D.; Iglesia, E. *J. Phys. Chem. B* **2001**, *105*, 5743.
- (41) Stoker, M. W. Phase Transformations in Fe Fischer–Tropsch Catalysts. Master Thesis, Brigham Young University, Provo, UT, 2000.
- (42) van der Kraan, A. M.; Nonnekens, R. C. H.; Stoop, F.; Niemants-verdriet, J. W. *Appl. Catal.* **1986**, *27*, 285.
- (43) Shroff, M. D.; Datye, A. K. *Catal. Lett.* **1996**, *37*, 101.
- (44) Davis, B. H. Determining Product Slates from Iron and Cobalt Catalysts. Center for Applied Energy Research, University of Kentucky, 2001.
- (45) Anderson, J. R. *Structure of Metallic Catalysts*; Academic Press: New York, 1975.
- (46) Guzzi, L. *Catal. Rev.—Sci. Eng.* **1981**, *23*, 329.
- (47) Bartholomew, C. H.; Stoker, M. W.; Mansker, L.; Datye, A. K. Effects of Pretreatment, Reaction, and Promoter on Microphase Structure and Fischer–Tropsch Activity of Precipitated Iron Catalysts. In *Catalyst Deactivation, 1999*; Delmon, B., Froment, G. F., Eds.; Studies in Surface Science and Catalysis; Elsevier Science: Amsterdam, 1999; Vol. 126, p 265.
- (48) Raupp, G. B.; Delgass, W. N. *J. Catal.* **1979**, *58*, 361.
- (49) Kovalchuk, V. I.; Kuznetsov, B. N. *J. Mol. Catal. A: Chem.* **1995**, *102*, 103.
- (50) Reymond, J. P.; Mériaudeau, P.; Teichner, S. J. *J. Catal.* **1982**, *75*, 39.
- (51) Datye, A. K.; Jin, Y.; Mansker, L.; Motjope, R. T.; Dlamini, T. H.; Coville, N. J. The nature of the active phase in iron Fischer–Tropsch catalysts. In *Studies in Surface Science and Catalysis*; Corma, A., Melo, F. V., Mendioroz, S., Fierro, J. L. G., Eds.; Elsevier: Amsterdam, 2000; Vol. 130, p 1139.
- (52) Jin, Y.; Datye, A. K. In *Natural Gas Conversion V*; Parmaliana, A., D. S., Frusteri, F., Vaccari, A., Arena, F., Eds.; Studies in Surface Science and Catalysis; Elsevier Science: Amsterdam, 1998; Vol. 119.
- (53) Clausen, B. S.; Topsøe, H. *Appl. Catal.* **1989**, *48*, 327.
- (54) Reymond, J. P.; Pommier, B.; Teichner, S. J. *Mechanism of the Fischer–Tropsch Synthesis on Iron Oxides*; Preprints: Division of Petroleum Chemistry, American Chemical Society: New York, 1986; Vol. 31.
- (55) Huang, C. S.; Ganguly, B.; Huffman, G. P.; Huggins, F. E.; Davis, B. H. *Fuel Sci. Technol. Int.* **1993**, *11*, 1289.
- (56) Eliason, S. A.; Bartholomew, C. H. *Appl. Catal., A* **1999**, *186*, 229.